

Joining of thin-walled tubes to sheets

João de Sousa Gameiro
joao.gameiro@ist.utl.pt

Instituto Superior Técnico, Lisboa, Portugal

October 2016

Abstract

This present paper draws from the fundamentals of sheet-bulk forming of thin-walled tubes to the proposal of a new joining process for fixing tubes to sheets by means of plastic deformation at room temperature. The new work on sheet-bulk forming of tubes is focused on local thickening (boss forming) by partial compression of the wall thickness along the longitudinal direction. The main goals are the understanding of the deformation mechanics of sheet-bulk forming of thin walled tubes and the characterization of its formability limits in terms of the major process parameters. The work on joining by forming investigates how local thickening can be successfully utilized for fixing tubes to sheets by mechanical locking with a flaring die. The overall work is supported by a numerical and experimental investigation and has the objective to widen and enhance the previous research in the field.

Keywords: Thin-walled tubes, Sheet-bulk forming, Joining by forming, Experimentation, Finite element modelling

1. Introduction

The utilization of sheet-bulk metal forming to produce functional components with local thickening and thinning can be analysed in two recent state-of-art reviews by Merklein [1] and by Mori and Nakano[2].

As can be concluded from these state-of-th-art reviews, the production of sheet metal parts by sheet-bulk forming (SBF) is more widespread than the production of tubular parts using the same technique. In fact, tubular parts are being fabricated by conventional spinning or by friction spinning with self-induced heat generation[3]. Another conclusion, is that major efforts in sheet-bulk technology have been mainly placed on the production of functional componentes by forming, despite its potential application in joining by forming[4].

This paper is aimed at exploring the potential application of SBF of thin-walled tubes in joining by forming. This new concept is different from the previous developments in joining of tubes[5] or joining of tubes to sheets[6]. Instead of making use of plastic instability waves which results in local buckling in tubes subjected to axial loading, now is being used sheet-bulk forming of tubes by partial compression of the wall thickness along the longitudinal direction for fixing tubes to sheets.

Unlike other proposed solutions[7, 8], which increases the thickness of the tube wall when facing a total compression, in this case, it is intended to pile-up material and obtain local thickening by partial compression of the wall thickness along the longitudinal direction in a press-tool system.

There are two major objetives for this paper. Firstly, and as the author is aware, it represents the first attempt to investigate the deformation mechanics of SBF of thin-walled tubes, as well as to identify and characterize its typical modes of deformation and to setup its formability limits as a function of the main process parameters. Secondly, taking advantage of localized thickening of the tube wall for subsequent joining of functional elements by forming. The new joining process for fixing tubes to sheets made of dissimilar materials is made by mechanical locking with a flaring die at room temperature. Finite element modelling and experimentation studies support the presentation and allow setting-up the workbility limits of the process in terms of major operating parameters.

To conclude,it is worth mentioning that the new proposed joint is adequate for applications where it is needed to ensure that the inner diameter of the joint is identical to that of the supplied tube. This requirement is not easy to achieve in case of mechanical joints obtained by fasteners or by propagation of plastic instability waves and may be of great importance in applications that convey fluids from one location to another in order to prevent changes in flow and pressure drops.

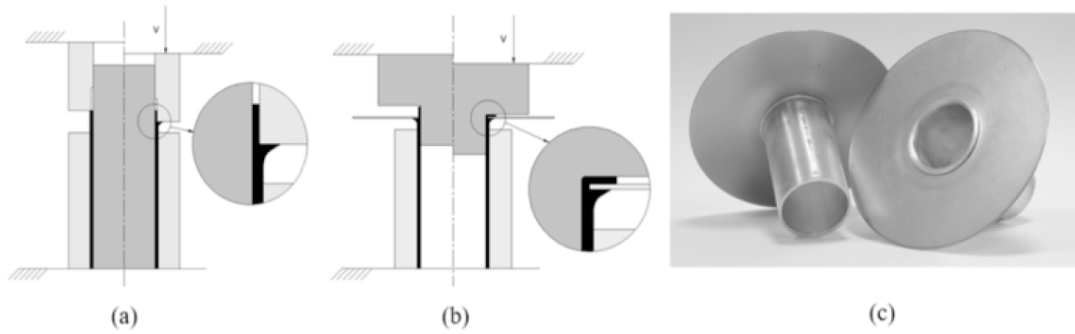


Figure 1: Sheet-bulk forming of thin-walled tubes for joining applications. (a) Schematic representation of material pile-up and localized thickening produced by partial compression of the wall thickness along the longitudinal direction. (b) Schematic representation of the procedure for flaring out (and locking) the upper tube end inserted in the sheet hole. (c) Hollow flanged components produced by the new proposed joining process.

2. Experimentation

2.1. Mechanical characterization of the material

The work on SBF of thin-walled tubes was performed on aluminum AA6063T6 tubes with an outer radius $r_0 = 16$ mm and a wall thickness $t_0 = 1.5$ mm.

The stress-strain curve of the material was determined by means of tensile and stack compression tests carried out at room temperature and following a procedure similar to the one done for tube branching by asymmetric compression beading[5]. The tests were on a hydraulic testing machine (Instron SATEC 1200 kN) with a cross-head speed equal to 10 mm/min and the resulting stress-strain curve is shown in Fig. 2.

$$\bar{\sigma} = 340.2\bar{\epsilon}^{0.158} \quad (1)$$

The critical instability force for the occurrence of local buckling was determined by compressing tubular specimens with 65 and 75 mm initial length between flat parallel platens. The tests were performed on the previously mentioned hydraulic testing machine with a cross-head speed equal to 10 mm/min and the tube end were neither laterally supported nor otherwise constrained. The resulting force displacement evolution is shown in Fig. 3 and the critical instability force F_{cr} for triggering local buckling is equal to 25.5 kN.

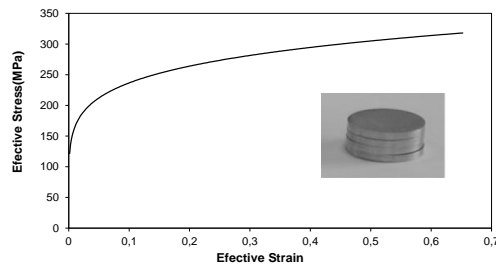


Figure 2: Stress-strain curve obtained from tensile and stack compression tests performed in specimens cut out from the supplied tubes.

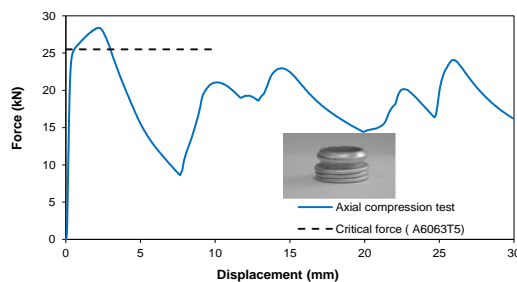


Figure 3: Force-displacement evolution and critical instability force for the axial compression of the supplied tubes between flat dies.

2.2. Tooling and work plan

The experimental work plan was split into two parts with different aims and objectives. The first part was exclusively focused on SBF of thin-walled tubes by partial compression of the wall thickness along the longitudinal direction. Fig. 4 presents a schematic representation of the initial and final positions of the tools with a detail showing the piled-up material at the final gap length l_{gap}^f between the upper and lower dies.

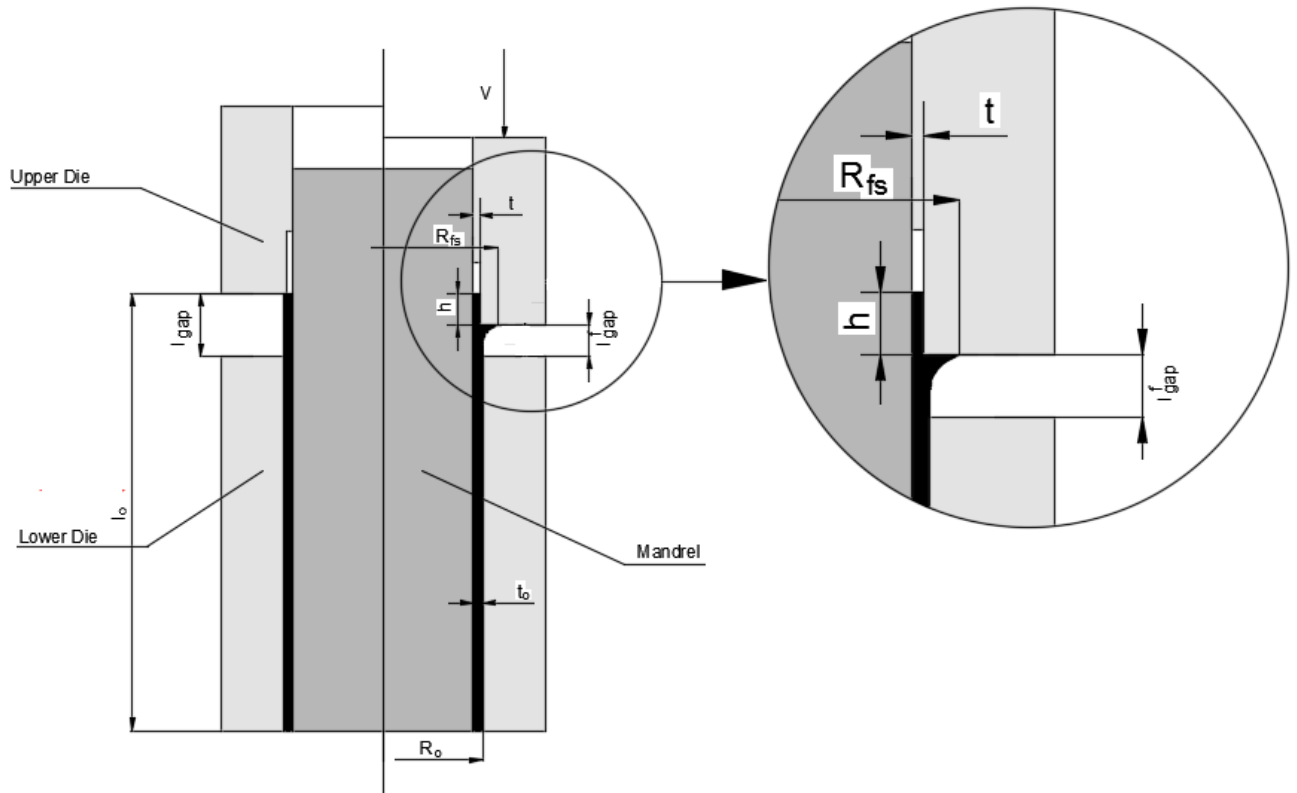


Figure 4: Main process parameters of the sheet-bulk forming of thin-walled tubes by partial compression of the wall thickness along the longitudinal direction.

The major parameters were identified as the following:

- The outer radius r_0 and wall thickness t_0 of the supplied tubes;
- The initial gap length l_{gap} between the upper and lower dies;
- The final gap length $l_{gap}^f = l_{gap} - h$, where h is the final piled-up length;
- The final wall thickness t resulting from the partial compression of the tube end along the longitudinal direction.

Table I summarizes the overall range of process parameters and only includes variations of two main process parameters because the outer radius r_0 and the wall thickness t_0 of the supplied tubes as well as the final gap length l_{gap}^f were kept unchanged. The reason for keeping it unchanged was to evaluate and compare the geometry of the piled-up material, namely the radius R_{fs} and final piled-up length h for different cases.

Table 1: The range of process parameters utilized in the experiments (nomenclature according to Fig.4).

r_0 (mm)	t_0 (mm)	l_{gap}^f (mm)	t (mm)	l_{gap} (mm)	l_0 (mm)
16	1.5	2	0.5-1.25	5-16	60-71

Regarding the second part of the experimental work plan, the main goal was to show its effectiveness in joining components made of dissimilar materials (Fig. 5a).

The key variable of this joining process is the corner radius r_c of the flaring die, which was taken as 0.3 mm (Fig.6a). Very small values of r_c ($r_c \cong 0$ mm) will give rise to a plastic instability and local buckling of the upper tube end, whereas large values of r_c ($r_c > t$) may induce bending in the sheet to be fixed to the tube. Both situations are unacceptable and shown in Fig. 4b and c.

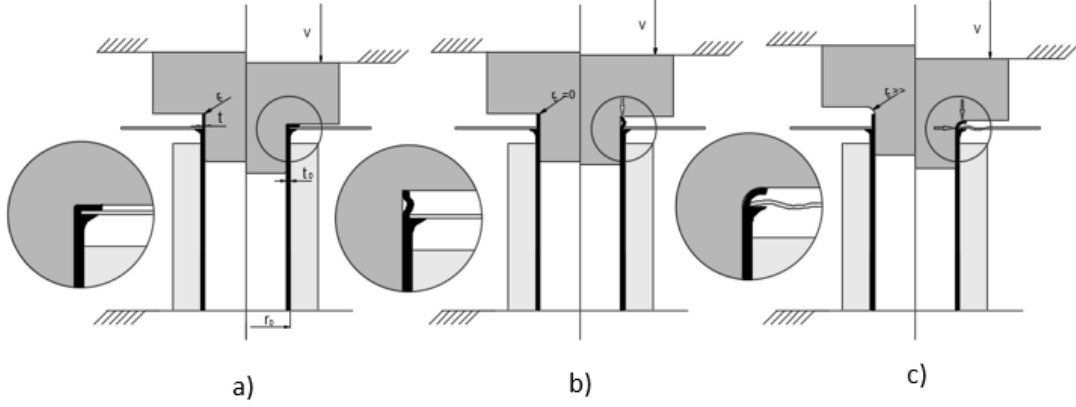


Figure 5: Fixing tubes to sheets by means of the new proposed joining process. (a) Mechanical locking by axial compression of the upper tube end with a flaring die. (b) Extreme situation resulting from the utilization of a very small corner radius of the upper flaring die. (c) Extreme situation resulting from the utilization of a very large corner radius of the upper flaring die.

3. Finite element modeling

Sheet-bulk forming of thin-walled tubes and the associated joining process for fixing tubes to sheets were simulated with an in-house computer program called I-Form. The program is based on the finite element formulation and accounts for the contact with friction between rigid and deformable objects,

$$\Pi = \int_V \bar{\sigma} \bar{\varepsilon} dV + \frac{1}{2} \int_V \dot{\varepsilon}_V^2 dV - \int_{S_T} T_i u_i dS + \int_{S_f} \left(\int_0^{|u^T|} \tau_f du_r dS + \frac{1}{2} P \sum_{c=1}^{N_c} (g_n^c)^2 + \frac{1}{2} P \sum_{c=1}^{N_c} (g_t^c)^2 \right) \quad (2)$$

In the above functional, the symbol $\bar{\sigma}$ denotes the effective stress, $\bar{\varepsilon}$ is the effective strain, $\dot{\varepsilon}$ is the volumetric strain rate, K is a large positive constant imposing the incompressibility of volume v , T_i and u_i are the surface tractions and velocities on surface S_T , τ_f and u_r are the friction shear stress and the relative velocity on the contact interface S_f between the tubes and tooling (dies and mandrels).

Friction is modelled through the utilization of the law of constant friction $\tau = m f$ and the friction factor m was set to 0.1 after checking the predicted forces that best matched the experimental results.

The last two terms in Eq. (2) are mainly relevant for the joining operation because they account for the contact with friction between the tube and the sheet to be joined. The interaction between these two deformable bodies is defined by N_c contact pairs that are identified by a two-pass node-to-segment algorithm, where the segments are the linear element sides of the quadrilateral elements. The symbols g_n^c and g_t^c denote the normal and tangential gap velocities in the contact pairs, which have to be penalized by a large number P in order to avoid penetration and to ensure full sticking between the counterfacing surfaces of the tubes and sheets to be joined. The penalization of the tangential gap velocity is omitted when simulating frictionless or frictional sliding. In case of frictional sliding, shear stresses are applied to the contacting surfaces through the third term of Eq. (2) which involves surface tractions T_i [9].

The finite element models that were utilized in the numerical modelling of both SBF of thin-walled tubes and joining of tubes to sheets took advantage of rotational symmetry conditions. Fig. 6 illustrates the discretization of the cross section of the tubes by means of linear quadrilateral elements with details showing the instants of time corresponding to the beginning and end of the SBF of thin-walled tubes.

The active tool components (dies and mandrel) were modelled as rigid objects and their geometries were discretized by means of contact- friction linear elements.

The overall central processing unit (CPU) time for a typical analysis shown in Fig. 6 with 10 intermediate remeshings was approximately equal to 30 min on a computer equipped with one Intel i7-5930 K CPU (3.5 GHz) processor.

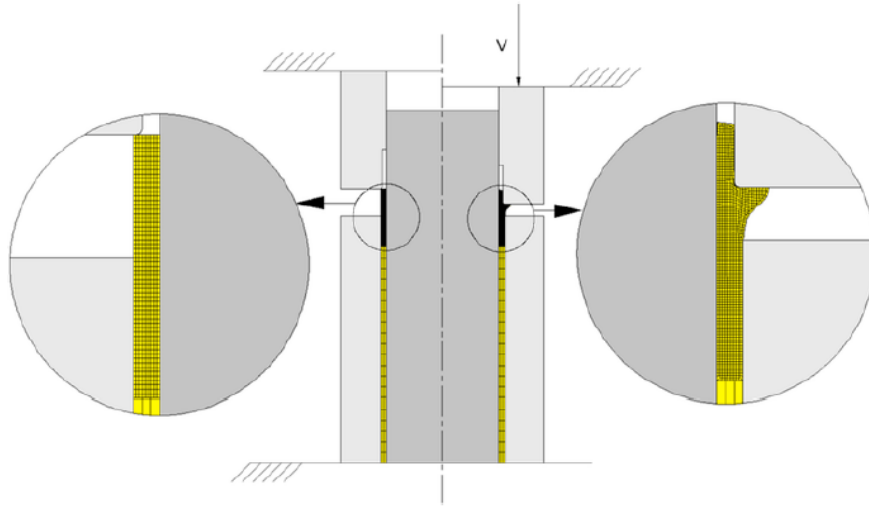



Figure 6: Finite element modelling of the sheet-bulk forming of thin-walled tubes at the initial and final instants of deformation.

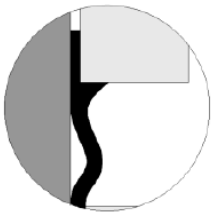
4. Results and discussion
4.1. Modes of deformation

In order to summarise the experimental results obtained in SBF of thin-walled tubes by partial compression of the wall thickness along the longitudinal direction for different initial gap lengths l_{gap} and final wall thicknesses t was created Table 2. The workability range corresponding to mode I is limited by the occurrence of local buckling in the original tube wall (mode II) or by cracking in the piled-up flange (mode III). The mode I* in Table 2 denotes a mode I with a very small piled-up length that is unsuitable for subsequent joining by forming.

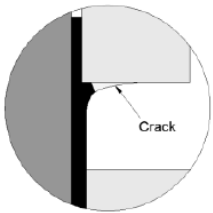
		l_{gap} (mm)								
		5	6	7	8	9	10	12	14	16
t (mm)	1.25	I	I	I	I	I	I	III	III	II
	1.0	I	I	I	I	I	II	II	II	II
	0.75	I*	I	I	II	II	II	II	II	II
	0.5	I*	I*	II	II	II	II	II	II	II



Mode I



Mode II



Mode III

Table 2

Summary of the experimentally observed modes of deformation as a function of the initial gap length l_{gap} and final wall thickness t .

Local buckling (mode II) is caused by plastic instability and its development is dependent on the slenderness ratio $\frac{l_{gap}}{t}$ between the initial gap length l_{gap} and the final wall thickness t . For values of the slenderness ratio $\frac{l_{gap}}{t} \geq 10$ the volume of piled-up material becomes very large and the compression forces increase beyond the critical instability force $F_{cr} = 25.5$ triggering local buckling. Fig.7 shows a picture and the corresponding finite element predicted geometry for a test case in which local buckling is clearly observed ($l_{gap} = 10\text{mm}$ and $t = 1\text{mm}$ present at Table 2).

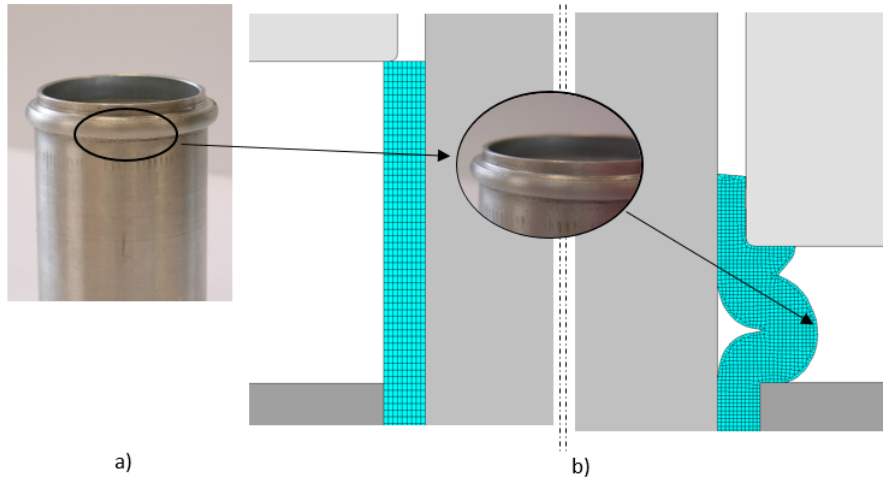


Figure 7: Local buckling caused by plastic instability in SBF of thin-walled tubes. (a) Photograph of a test case with $l_{gap} = 10$ mm and $t = 1$ mm. (b) Initial mesh and finite element predicted geometry for the test case shown in (a).

Cracks along the outer radius R_{fs} of the piled-up flange open by circumferential σ_0 tensile stresses and are triggered by the accumulation of damage beyond a critical threshold value. Fig. 8 shows a picture and the corresponding finite element predicted distribution of accumulated damage according to the triaxiality based criterion due to Mc Clintock (1968). The test case is at Table 2 and corresponds to a $l_{gap} = 14$ mm and $t = 1.25$ mm, and the largest value of accumulated ductile damage is registered at the outer radius R_{fs} where the cracks appear.

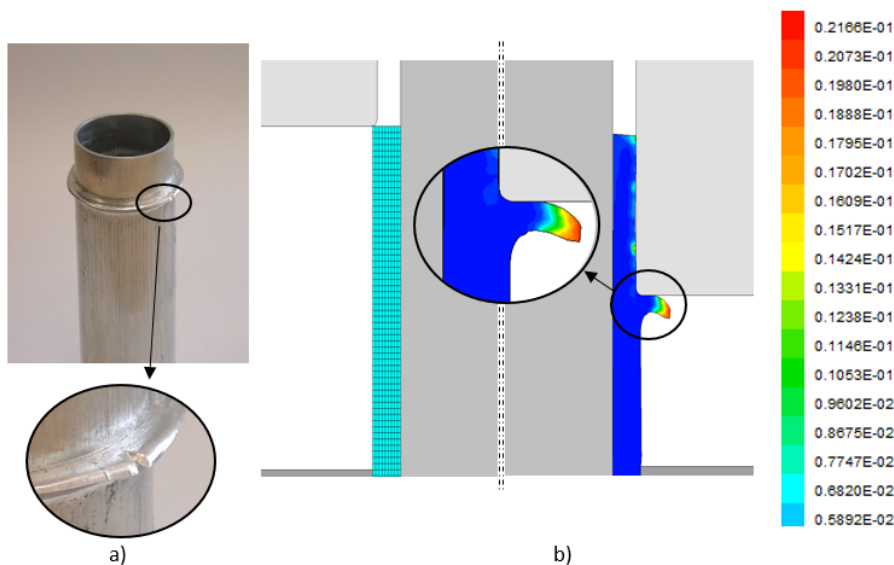


Figure 8: Cracking of the outer radius of the piled-up flange in SBF of thin-walled tubes. (a) Photograph of a test case with $l_{gap} = 14$ mm and $t = 1.25$ mm. (b) Initial mesh and final element predicted accumulation of ductile damage according to McClintock (1968) triaxiality based criterion for the test case shown in (a).

Fig.9 shows a picture corresponding to the test cases of the first line of Table 2 where is possible to identify the different modes of deformation and how they evolve with the increase of the initial gap length l_{gap} .



Figure 9: Modes of deformation for a set of test cases in which the final wall thickness $t = 1.25$ mm and the initial gap length l_{gap} varies from 5 to 16 mm (first row in Table 2).

In terms of joining, it is important to ensure that the radius R_{fs} of the piled-up flange and the final piled-up length h are big enough for fixing the sheets to the tubes by flaring out and locking the upper tube end inserted in the sheet hole. For the first parameter, small values of R_{fs} are unable to guarantee a wide bearing surface that reduces the chance of the tube being pull-out. For the second, small values of h are inadequate for flaring out the upper tube end and ensure a mechanical lock with the sheet.

Fig.10 and Fig.11 show the experimental evolution of the radius R_{fs} of the pile-up flange and the the final piled-up length h with the initial gap length l_{gap} for a fixed value of the final gap length $l_{gap}^f = 2$ mm.

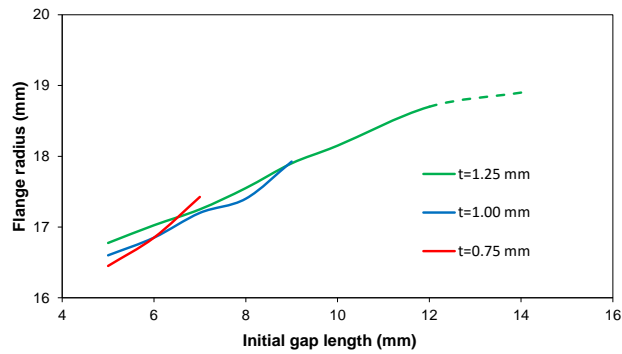


Figure 10: Evolution of outer radius R_{fs} of the piled-up flange with the initial gap length l_{gap} in SBF of thin-walled tubes.

As seen, R_{fs} increases in a quasi-linear manner with l_{gap} as a result of the growing volume of the piled-up material up to the critical gap length where local buckling (mode II) develops as a result of plastic instability. The dashed lines in Fig.10 correspond to results obtained from test cases in which mode III is triggered before mode II.

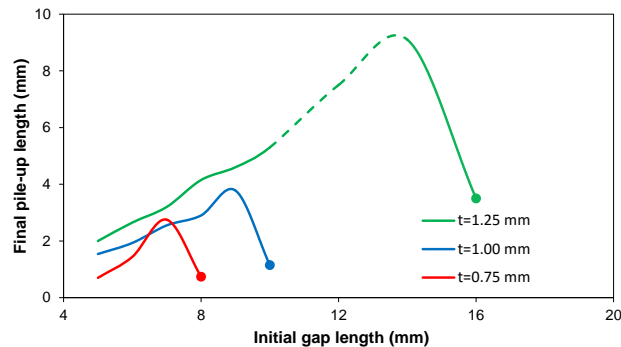


Figure 11: Evolution of the final piled-up length h with the initial gap length l_{gap} in SBF of thin-walled tubes.

For the case of h , Fig.11 shows that this value increases until it reaches its maximum, which represents the moment from which the phenomenon of local buckling occurs, the filled circle represents it. The dashed line corresponds to mode III, in which despite the occurrence of cracks, it maintains the increase value of h .

4.2. Compression force

Fig.12 shows the experimental and finite element predicted evolution of the force displacement in SBF of thin-walled tubes by partial compression of the wall thickness along the longitudinal direction. The selected cases included in the figure were taken from Table 2 and correspond to deformation mode I ($l_{gap}=7$ mm and $t=0.75$ mm) and II ($l_{gap}=10$ mm and $t=1$ mm).

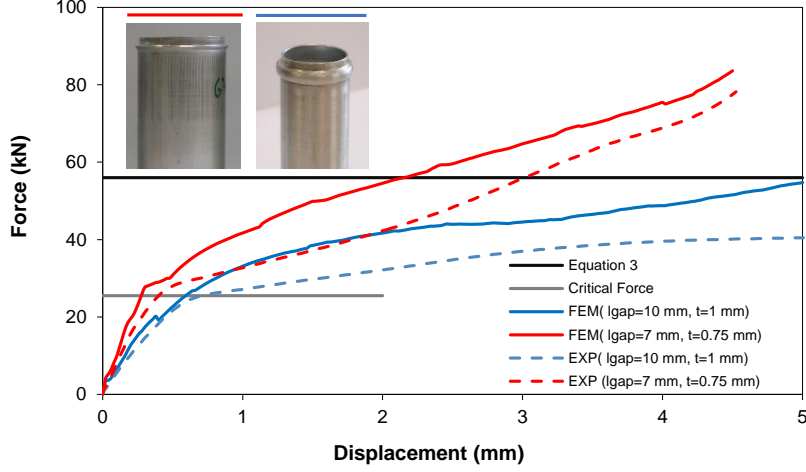


Figure 12: Evolution of the compression force with displacement in SBF of thin-walled tubes.

As seen, the force increases steeply from zero up to a value close to the critical instability force $F_{cr}=25.5$ kN for the selected test case corresponding to mode I and more gradually for the selected test case corresponding to mode II. The reason for this different behavior is due to the need of attaining a larger piled-up length of reaching the same amount of force when the final wall thickness t is larger.

The test case corresponding to mode I presents a stable monotonic growth similar to that commonly observed in the transition from forming to steady-state cutting in orthogonal metal cutting[10]. In contrast, the test case corresponding to mode II presents an evolution towards near constant force as a result of local buckling under a decreasing free gap length.

The maximum SBF force in mode I may be compared with the cutting force after reaching steady-state conditions. It was estimated by considering an 'equivalent' orthogonal metal cutting model with an undeformed chip thickness $e = t_0 - t$ and a chip width $w = 2\pi r_0$, where t_0 , t , r_0 are defined in accordance to Fig.4,

$$F_c = k_s e w = 2k_s \pi r_0 (t_0 - t) \quad (3)$$

The symbol k_s denotes the specific cutting pressure, which may be taken as 750 MPa for typical aluminium alloys with an undeformed chip thickness equal to 0.75 mm/rev[11].

The main reason why the compression force in SBF of thin-walled tubes is higher than that of the 'equivalent' orthogonal metal cutting model (Fig.12) is because there is no transition from forming to cutting due to the absence of material separation at the upper die tip. In fact, the axisymmetric circumferential constraint of the piled-up flange prevents chip formation, and the reason why critical accumulation of damage takes place at the outer flange radius instead of the upper die tip, may also be understood as the way material acts to eliminate the circumferential constraint that prevents chips to form.

4.3. Joining by forming

The last section of this paper is focused on fixing the sheet-bulk formed tubes to sheets by mechanical locking with a flaring die. Fig.14a shows the finite element predicted geometry of a joint made from an AA6063T6 tube and DC04 sheet, in which the upper tube end was previously shaped by partial sheet-bulk compression of the wall thickness along the longitudinal direction ($l_{gap}=7$ mm and $t=1$ mm). The results prove the feasibility of the proposed joining process and confirm the adequacy of using a corner radius r_c of the upper die equal to a 0.3 mm.

In contrast, the results shown in Fig.14b and c show the inadequacy of using very small or large corner radius r_c of the flaring die due to the risk of triggering plastic instability of the upper tube end (case b) or bending along the sheet to be fixed (case c).

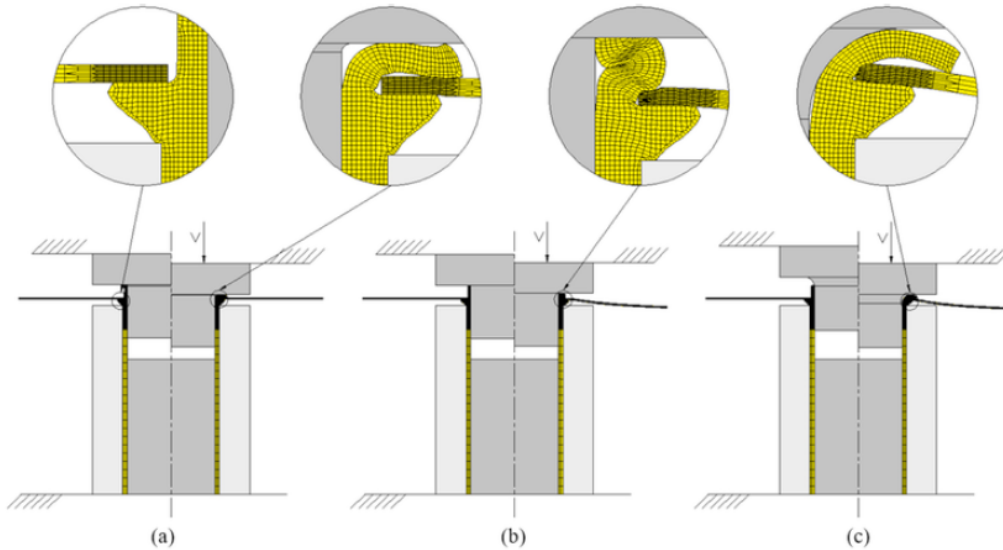


Figure 13: Joining sheet-bulk formed tubes ($l_{gap} = 7$ mm and $t = 1$ mm) to sheets by flaring out (and locking) the upper tube end inserted in the sheet hole. (a) Finite element predicted geometry of a sound joint obtained with a corner radius of the upper flaring die $r_c = 0.3$ mm. (b) Finite element predicted geometry of an inadmissible joint produced with an upper flaring die without corner radius ($r_c = 0$ mm). (c) Finite element predicted geometry of an inadmissible joint produced with an upper flaring die with a very large corner radius ($r_c = 3$ mm).

Fig. 15 gives insight into the mechanical strength of the new proposed joint by providing a experimental and numerical estimate of the maximum compression that the joint is capable of withstanding during a destructive tensile test. As seen, up to a force of approximately 2.5 kN the mechanical joint remains practically unchanged. However, once the mechanical starts to yield, there is a maximum tensile force (approximately 3 kN) after which deformation continues up to failure by loosening of the mechanical lock between the tube and sheet.

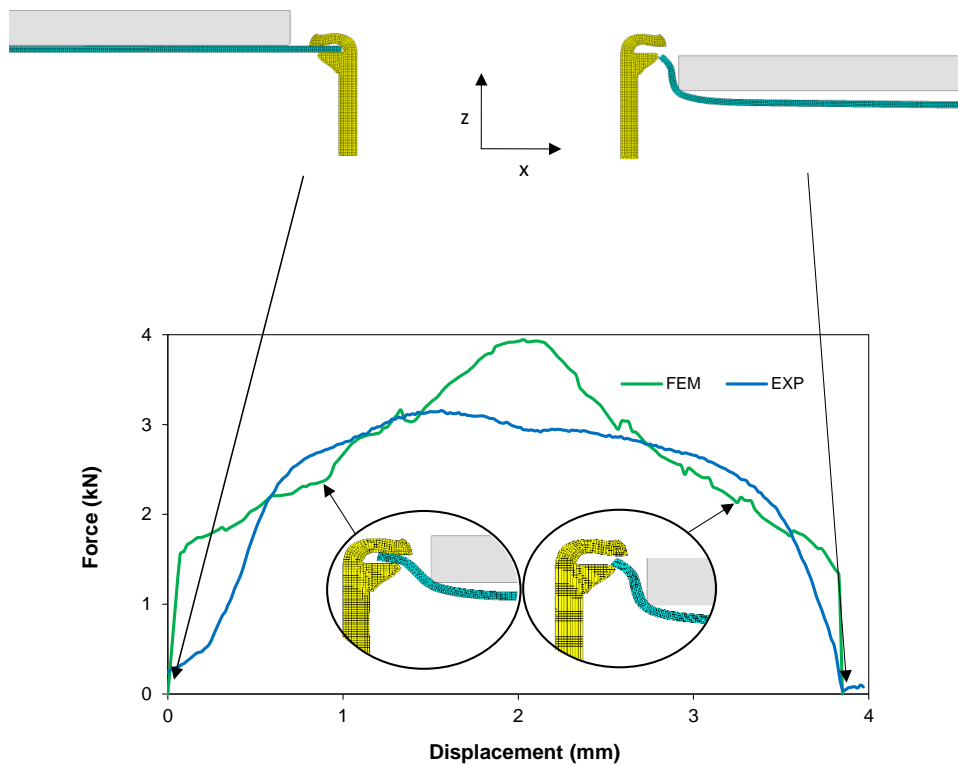


Figure 14: Finite element modelling a destructive tensile test performed on a sound joint ($l_{gap} = 7$ mm, $t = 1$ mm and $r_c = 0.3$ mm) with the predicted evolution of the force with displacement.

5. Conclusions

Sheet-bulk forming of tubes by partial compression of the wall thickness is employed to pile-up material along the longitudinal direction.

The process can be utilized to produce functional tubular parts with localized circumferential thickening for various applications such as fixing tubes to sheets by mechanical locking.

The deformation mechanics of the sheet-bulk forming of tubes is limited by the occurrence of plastic instability and buckling for ratios $\frac{l_{gap}}{t} \geq 10$ between the initial gap length l_{gap} and the final wall thickness t . Radial cracks along the outer radius of the piled-up material can also develop due to the accumulation of ductile damage in cases with large values of initial gap length l_{gap} .

The combination of sheet-bulk forming with flaring of the upper tube end allows fixing tubes to sheets made from dissimilar materials, at room temperature. The process is mainly limited by the corner radius r_c of the flaring die because inexistent corner radius ($r_c \cong 0$ mm) will give rise to plastic instability of the upper tube end whereas large corner radius ($r_c = 3$ mm) will bend the sheet along its radius. In between these two limiting conditions it is possible to produce sound fixtures of tubes to sheets.

References

- [1] M Merklein, JM Allwood, B-A Behrens, A Brosius, H Hagenah, K Kuzman, K Mori, AE Tekkaya, and A Weckenmann. Bulk forming of sheet metal. *CIRP Annals-Manufacturing Technology*, 61(2):725–745, 2012.
- [2] K Mori and T Nakano. State-of-the-art of plate forging in japan. *Production Engineering*, 10(1):81–91, 2016.
- [3] Werner Homberg and Daniel Hornjak. Friction spinning—new innovative tool systems for the production of complex functionally graded workpieces. In *THE 14TH INTERNATIONAL ESAFORM CONFERENCE ON MATERIAL FORMING: ESAFORM 2011*, volume 1353, pages 177–182. AIP Publishing, 2011.
- [4] Ken-ichiro Mori, Niels Bay, Livan Fratini, Fabrizio Micari, and A Erman Tekkaya. Joining by plastic deformation. *CIRP Annals-Manufacturing Technology*, 62(2):673–694, 2013.
- [5] LM Alves and PAF Martins. Tube branching by asymmetric compression beading. *Journal of Materials Processing Technology*, 212(5):1200–1208, 2012.
- [6] Adriano Gonçalves, Luis M Alves, and Paulo AF Martins. Inclined tube-sheet plastically deformed joints. *steel research international*, 85(1):67–75, 2014.
- [7] Peter Sieczkarek, Lukas Kwiatkowski, Nooman Ben Khalifa, and A Erman Tekkaya. Novel five-axis forming press for the incremental sheet-bulk metal forming. In *Key Engineering Materials*, volume 554, pages 1478–1483. Trans Tech Publ, 2013.
- [8] Marion Merklein, A Erman Tekkaya, Alexander Brosius, Simon Opel, Lukas Kwiatkowski, Björn Plugge, and Sebastian Schunk. Machines and tools for sheet-bulk metal forming. In *Key Engineering Materials*, volume 473, pages 91–98. Trans Tech Publ, 2011.
- [9] Chris Valentin Nielsen, Wengi Zhang, LM Alves, Niels Bay, and Paulo Martins. *Modeling of thermo-electro-mechanical manufacturing processes: applications in metal forming and resistance welding*. Springer Science & Business Media, 2012.
- [10] PAR Rosa, O Kolednik, PAF Martins, and AG Atkins. The transient beginning to machining and the transition to steady-state cutting. *International Journal of Machine Tools and Manufacture*, 47(12):1904–1915, 2007.
- [11] Tungaloy. *Cutting Tools*. IMC Group. 2013.